DOI: 10.1002/asia.200600252

Thermotropic Liquid Crystals Based on Extended 2,5-Disubstituted-1,3,4-Oxadiazoles: Structure–Property Relationships, Variable-Temperature Powder X-ray Diffraction, and Small-Angle X-ray Scattering Studies

Jie Han, Stephen Sin-Yin Chui, and Chi-Ming Che*[a]

Abstract: A class of extended 2,5-disubstituted-1,3,4-oxadiazoles R^1-C_6H_4-{OC_2N_2}-C_6H_4-R^2 ($R^1 = R^2 = C_{10}H_{21}O$ **1a**, *p*-$C_{10}H_{21}O$-C_6H_4-C≡C **3a**, *p*-CH_3O-C_6H_4-C≡C **3b**; $R^1 = C_{10}H_{21}O$, $R^2 = CH_3O$ **1b**, $(CH_3)_2N$ **1c**; F **1d**; $R^1 = C_{10}H_{21}O$-C_6H_4-C≡C, $R^2 = C_{10}H_{21}O$ **2a**, CH_3O **2b**, $(CH_3)_2N$ **2c**, F **2d**) were prepared, and their liquid-crystalline properties were examined. In CH_2Cl_2 solution, these compounds displayed a room-temperature emission with λ_{max} at 340–471 nm and quantum yields of 0.73–0.97. Compounds **1d**, **2a**–**2d**, and **3a** exhibited various thermotropic mesophases (monotropic, enantiotropic nematic/smectic), which were examined by polarized-light optical microscopy and differential scanning calorimetry. Structure determination by a direct-space approach using simulated annealing or parallel tempering of the powder X-ray diffraction data revealed distinctive crystal-packing arrangements for mesogenic molecules **2b** and **3a**, leading to different nematic mesophase behavior, with **2b** being monotropic and **3a** enantiotropic in the narrow temperature range of 200–210 °C. The structural transitions associated with these crystalline solids and their mesophases were studied by variable-temperature X-ray diffractometry. Nondestructive phase transitions (crystal-to-crystal, crystal-to-mesophase, mesophase-to-liquid) were observed in the diffractograms of **1b, 1d**, **2b, 2d**, and **3a** measured at 25–200 °C. Powder X-ray diffraction and small-angle X-ray scattering data revealed that the structure of the annealed solid residue **2b** reverted to its original crystal/molecular packing when the isotropic liquid was cooled to room temperature. Structure–property relationships within these mesomorphic solids are discussed in the context of their molecular structures and intermolecular interactions.

Keywords: liquid crystals · materials science · mesophases · phase transitions · X-ray diffraction

Introduction

The search for new liquid-crystal materials continues to be an area of advanced technological importance owing not only to their application in liquid-crystal-display devices[1] and as light modulators[2] and switches,[3] but also to their electrically controlled birefringence (ECB).[4] The incorporation of tunable luminescent properties into mesomorphic materials has led to the construction of a new generation of mesogens for use in the construction of efficient light emitters and charge carriers for electroluminescent (EL) devices.[5] In this regard, rational molecular design and synthesis studies are crucial for the continued development of new molecular materials that have unique or interesting supramolecular architectures and liquid-crystal-display properties. The formation of simple neutral organic molecules or salts by self-assembly, leading to the construction of various mesomorphic structures, has been extensively studied over the past decade.[6] In particular, the orientational flexibility and molecular anisotropy of mesogens have been utilized to alter the optoelectronic performance of a number of liquid-crystal-based devices, owing to their facile self-organized supramolecular aggregation with various noncovalent intermolecular interactions.[7]

Liquid-crystal materials based on derivatives of 2,5-diphenyl-1,3,4-oxadiazole have been studied, and various polymers and dendrimers containing this structural motif have been prepared.[8] Compounds with the 1,3,4-oxadiazole motif are generally chemically stable and have diverse luminescent properties, and are often emissive mesogens with good electron-transport properties.[9] Although the crystal

[a] Dr. J. Han, Dr. S. S.-Y. Chui, Prof. C.-M. Che
Department of Chemistry and the
HKU-CAS Joint Laboratory on New Materials
The University of Hong Kong
Pokfulam Road, Hong Kong (China)
Fax: (+852) 28571586
E-mail: cmche@hku.hk

Supporting information for this article is available on the WWW under http://www.chemasianj.org or from the author.

structures of nonmesogenic 2,5-disubstituted-1,3,4-oxadiazoles with different functionalities have been reported,[10] structural information on mesogenic materials containing 2,5-diaryl-1,3,4-oxadiazole is lacking, owing to difficulties in obtaining single crystals suitable for X-ray diffraction studies.[11a–d] To the best of our knowledge, related studies on extended 2,5-diaryl-1,3,4-oxadiazoles are less-explored.[11e] Herein, a new family of extended calamitic (rodlike) mesogenic molecules were synthesized (Scheme 1) by changing the mesogen core lengths and terminal substituents. Their liquid-crystal properties were analyzed by polarized optical microscopy (POM) and the phase transitions associated with these mesogenic compounds were studied by differential scanning calorimetry (DSC) and variable-temperature X-ray diffractometry (VTXRD). Notably, structure determination by a direct-space approach using simulated annealing (DASH) or parallel tempering (FOX) of the powder X-ray diffraction (XRD) data of mesogenic molecules **2b** and **3a** revealed distinctive crystal packing. Small-angle X-ray scattering (SAXS) investigations were used to reveal changes in long-range molecular order for these extended mesomorphic compounds that were annealed below their decomposition temperatures.

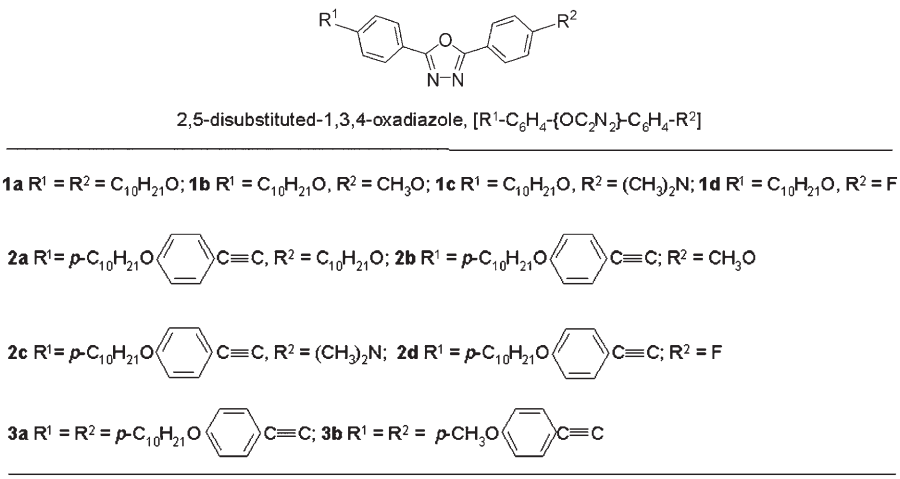

Scheme 1. Molecular structures of **1**–**3**.

Results and Discussion

Synthesis and Characterization

Scheme 1 shows the structures of compounds **1**–**3** studied herein. Details of the synthesis and characterization of the materials are given in the Supporting Information. Compounds **1a**–**1d** were prepared in good yields according to literature methods with minor modifications,[15] whereas compounds **2a**–**2d**, **3a**, and **3b** were prepared from 2-(phenylethynyl)-5-(phenyl)- or 2,5-(diphenylethynyl)-1,3,4-oxadiazoles and 1-iodo-4-decyloxybenzene by a Pd/Cu^{I}-catalyzed coupling reaction.[16] 2,5-Disubstituted-1,3,4-oxadiazoles were prepared by the cyclization of aldehyde hydrazones[17a] or the reaction of tetrazoles with acid chlorides (Huisgen route).[17b] A small number of studies on extended 2,5-diaryl-1,3,4-oxadiazoles containing a C≡C linkage were recently reported.[11e,18] The incorporated C≡C linkages not only enable the linear extension of mesogen length but also serve as acceptors in noncovalent C–H···π(C≡C) interactions. Extensive studies reporting the applications of C–H···π(C≡C) interactions in crystal engineering and metal–organic coordination chemistry have been reviewed elsewhere.[19]

Crystal Structure of IIIc and Vc

During the synthesis of **2c**, crystals of the intermediates **IIIc** (2-(4-iodophenyl)-5-(4-*N*,*N*′-dimethylphenyl)-1,3,4-oxadiazole) and **Vc** (2-(4-ethynylphenyl)-5-(4-*N*,*N*′-dimethylphenyl)-1,3,4-oxadiazole) suitable for X-ray crystal-structure determination[20] were obtained by slow evaporation of solutions in hexane and CH_2Cl_2, respectively. As shown in Figure 1, both compounds adopt a nearly planar molecular structure.

Abstract in Chinese:

本文合成了一系列 2,5-二芳基取代-1,3,4-噁二唑类新化合物，其结构为： R^1-C_6H_4-{OC_2N_2}-C_6H_4-R^2 (R^1 = R^2 = $C_{10}H_{21}O$ **1a**; *p*-$C_{10}H_{21}O$-C_6H_4-C≡C **3a**; *p*-CH_3O-C_6H_4-C≡C **3b**) 及 (R^1 = $C_{10}H_{21}O$, R^2 = CH_3O **1b**; $(CH_3)_2N$ **1c**; F **1d**; R^1 = $C_{10}H_{21}O$-C_6H_4-C≡C, R^2 = $C_{10}H_{21}O$ **2a**; CH_3O **2b**; $(CH_3)_2N$ **2c**; F **2d**)。研究了该类化合物的液晶性能及在溶液中的荧光性能。 在室温下，这些化合物的二氯甲烷溶液的最大荧光发射波长λ_{max}为 340-371nm，荧光量子产率ϕ=0.73-0.97。偏光显微镜（POM）及差示扫描量热分析（DSC）结果表明化合物 **1d**, **2a-2d** 及 **3a** 具有不同的液晶相（单变或互变的向列相或近晶 A 相）。依据粉末 X 射线衍射（PXRD）数据，采用从头计算法进行分子结构研究发现化合物 **2b** 及 **3a** 具有不同的晶体分子堆积方式，这使它们具有不同的液晶态，**2b** 为单变的向列相液晶，而 **3a** 在 200-210 °C 之间具有互变的向列相。通过变温 X 射线衍射 (VT-XRD) 研究了化合物 **1b, 1d, 2b, 2d** 和 **3a** 在 25-200 °C 之间进行升降温过程中晶态与液晶态转变的结构变化（晶态→晶态，晶态→液晶态，液晶态→液态），VT-XRD 数据与 POM 和 DSC 测试结果一致。粉末 X 射线衍射及小角 X 射线散射 (SAXS) 研究发现化合物 **2b** 从熔融的各向同性液体冷却到室温得到的固体与初始的分子堆积方式相同。本文还详细讨论了分子结构及分子间作用力与液晶性和荧光性之间的关系。

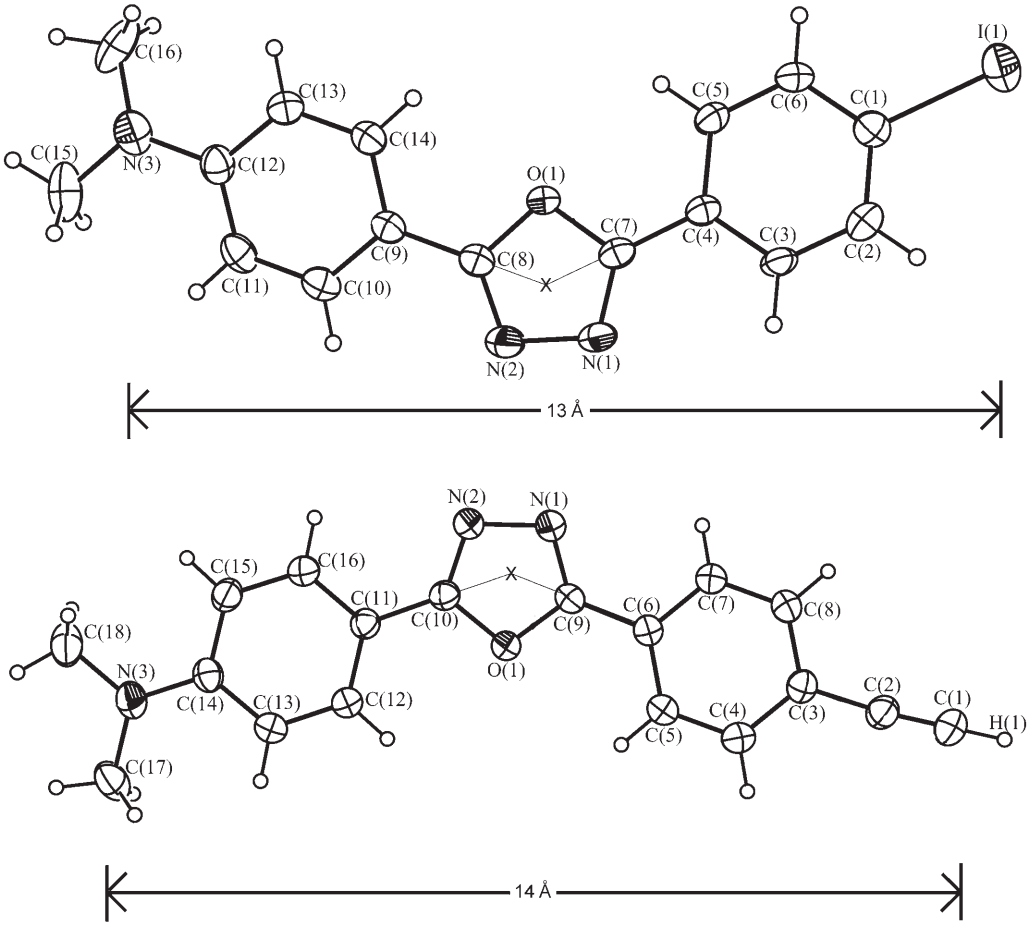

Figure 1. ORTEP diagrams of **IIIc** (top) and **Vc** (bottom) showing their estimated molecular sizes, bending angles (C(8)–X–C(7) = 134° for **IIIc**, C(10)–X–C(9) = 140°; X = centroid of oxadiazole ring) and dihedral angles (C(14)–C(9)–C(8)–O(1) = −7.03°, C(5)–C(4)–C(7)–O(1) = −7.06° for **IIIc**; C(12)–C(11)–C(10)–O(1) = 4.31°, C(5)–C(6)–C(9)–O(1) = −7.00° for **Vc**).

Crystal Packing of 2b and 3a

It is generally difficult to obtain single crystals of mesogenic compounds suitable for XRD studies. Herein, we were able to estimate the molecular length and conformation of the 2,5-diphenyl-1,3,4-oxadiazole moiety from the crystal structures of **IIIc** and **Vc**. The extended molecules **2b** and **3a** were constructed by adding the *n*-decyl chain(s) or methoxy substituents to the bent 2,5-diphenyl-1,3,4-oxadiazole moiety. By assuming 1) a molecular length of 6.4 Å for each phenylethynyl motif and 2) that the methylene groups of the *n*-decyl chain in **2b** and **3a** adopt an all-*trans* configuration with an average size of 1.15–1.20 Å per CH_2 unit,[21] the estimated molecular length for molecules **2b** and **3a** are 30 Å and 47 Å, respectively (Figure 2). In the diffractograms of **2b** and **3a**, the diffraction peak maxima displayed periodic trends [q, $2q$, $3q$, $4q$, $5q$ where $q \propto \sin 2\theta$; q/Å^{-1} (2θ/°) values: 0.046 (2.647), 0.069 (4.007), 0.094 (5.401), 0.117 (6.756), 0.141 (8.118) for **2b** (the first peak is out of the detection limit ($2\theta_{min} = 3.0°$) of the diffractometer); 0.030 (1.708), 0.061 (3.520), 0.093 (5.337), 0.124 (7.146), 0.155 (8.944) for **3a**] indicative of layered structures with definite lamellar thickness. Indexing the room-temperature diffractograms of **2b** and **3a** revealed the coexistence of long and short unit-cell edges. Rietveld profile fitting of the powder XRD data followed by restrained structural refinement gave

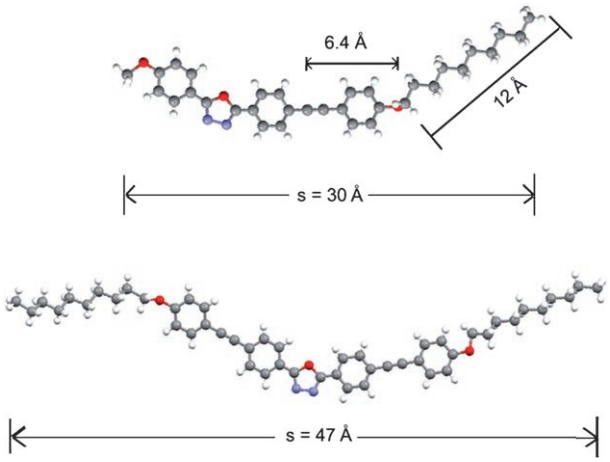

Figure 2. Molecular models of **2b** (top) and **3a** (bottom) with estimated lengths.

CHEMISTRY
AN ASIAN JOURNAL

the structural parameters summarized in Table 1. The graphical plots calculated after Rietveld profile refinement of the data obtained for **2b** and **3a** are given in the Supporting Information.

Table 1. Structural refinement data for **2b** and **3a**.

	2b	**3a**
Crystal system	Monoclinic	Monoclinic
Space group	$P2_1/c$	$P2_1/c$
a [Å]	66.12(2)	49.69(2)
b [Å]	5.182(1)	4.761(2)
c [Å]	8.014(2)	17.008(5)
β [°]	103.18(3)	94.12(6)
V [Å^3]	2673.7	4013.2
M_r	508.6	735.02
ρ [g cm^{-3}]	1.264	1.217
2θ [°]	1.5-50	1.5-40
Reflections	937	707
Variables	274	390
Restraints	214	335
R_p[a]	0.095	0.079
R_{wp}[a]	0.132	0.107
R_{wp} (expected)[a]	0.108	0.074
R_F[b]	0.105	0.108
Goodness of fit	2.77	2.93
Max. (shift/esd)^2 (mean)	0.22 (0.02)	0.26 (0.03)

[a] $R_p=\Sigma_i|y_{i,o}-y_{i,c}|/\Sigma_i|y_{i,o}|$; $R_{wp}=[\Sigma_i w_i(y_{i,o}-y_{i,c})^2/\Sigma_i w_i(y_{i,o})^2]^{1/2}$; expected $R_{wp}=R_{wp}/\chi^2$; $\chi^2=\Sigma_i w_i(y_{i,o}-y_{i,c})^2/(N_{obs}-N_{var})$; $y_{i,o}$ and $y_{i,c}$ are the observed and calculated intensities at point i of the profile, respectively, N_{obs} is the number of theoretical Bragg peaks in the 2θ range, N_{var} is number of the refined parameters. Statistical weights w_i are normally taken as $1/y_{i,o}$. [b] $R_F=\Sigma|I_{jobs}^{1/2}-I_{jcalcd}^{1/2}|/\Sigma I_{jobs}^{1/2}$; I_j denotes the intensity assigned to the jth Bragg reflection.

Figure 3 shows the crystal packing for **2b** viewed along the [010] direction. The long edge (66 Å) of the unit cell is 2.2 times longer than the molecular length (30 Å), thus leading to the formation of bilayer lamellar structures. The long axis of each molecule is parallel to the long edge of the unit cell. The imposed symmetry constraints of the space group $P2_1/c$ indicate a parallel molecular arrangement with head-to-head and tail-to-tail orientations. The lateral molecular order is also formed in the *ac* plane of the crystal structure, as revealed by the prominent diffraction maxima at 24.5° (2θ) (or $d=3.67$ Å). This interplanar distance d is consistent with the expected molecular width of **2b**. Extensive hydrophobic interactions (average C···C distances > 4.0 Å) among the *n*-decyl chains and intermolecular C–H···O interactions (C(29)–H(29)···O(27) = 2.271 Å, C(38)–H(38)···O(1) = 2.404 Å) were also observed.

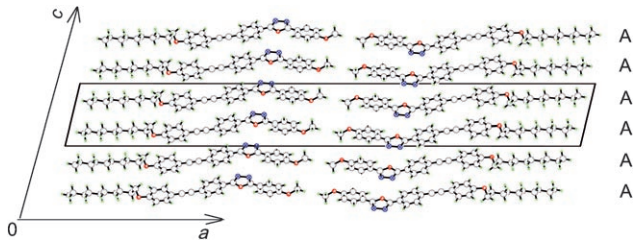

Figure 3. Crystal packing of **2b** viewed along the [010] direction showing head-to-head and tail-to-tail molecular orientations stacked in an "AAAAAA" fashion.

The more-extended mesogenic molecule **3a** crystallized in the same space group as **2b**, but formed a different lamellar structure. Figure 4 shows the crystal packing of molecules of **3a** along the [010] direction. The long edge (49.6 Å) of the unit cell is close to the length (47 Å) of the molecule. Unlike the case of **2b**, the *c*-glide translational symmetry (x, y, $z\rightarrow x$, $y-{}^1/_2$, $z+{}^1/_2$) indicates that there are alternating molecular stacks of **3a** along the *c* axis, forming a distinctive ABABAB molecular-stacking sequence.

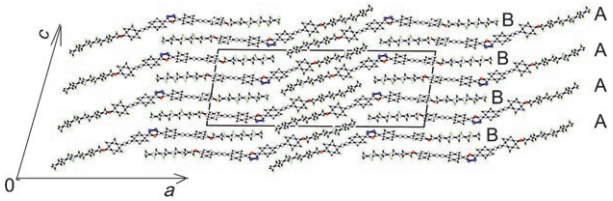

Figure 4. Crystal packing of **3a** viewed along the *b* axis showing alternating molecular stacks with an ABABABAB sequence.

The crystal structures and molecular-packing arrangements of **2b** and **3a** can be used to model the solid-state structures for **1d** and **2d**. In the diffractograms obtained for **1d** and **2d**, the periodicity of diffraction peak maxima (2θ) [q, $2q$, $3q$, $4q$, $5q$; q/Å^{-1}(2θ/°): 0.041 (2.347), 0.083 (4.756), 0.125 (7.170), 0.166 (9.579), 0.208 (12.022) for **1d**; 0.033 (1.877), 0.067 (3.823), 0.097 (5.560), 0.135 (7.803), 0.168 (9.685) for **2d**] indicates layered structures with lamellar thicknesses of 37.6 Å and 47.0 Å, respectively, as was found for **2b**. These lamellar thicknesses are longer than the respective estimated molecular lengths (23.5 Å for **1d** and 30 Å for **2d**), showing that **1d** and **2d** most likely adopt similar staggered bilayer structures but with slightly altered molecular orientations. The proposed crystal packing for **1d** (and **2d**) is shown in Scheme 2, based on the estimated molecular length of 23.5 Å for **1d** and 30 Å for **2d**. All these mesogenic molecules are aligned with tilting angles of about 37° (or 53° away from the normal of the molecular stacks). We attribute this result to supramolecular self-assembly through intermolecular C–H···F–C hydrogen bonding between neighboring *p*-fluorophenyl groups.[22] Furthermore, the prominent diffraction maxima at 24.5° and 28° (2θ) in the diffractogram of **2d** indicate that the lateral molecular order is similar to that found for **2b** and **3a**. However, there is a lack of defined periodicity in the diffraction peak maxima for **1b**, precluding the existence of a lamellar structure.

Electronic Absorption and Emission Spectroscopy

The UV/Vis absorption and emission data for solutions of **1a–3b** in CH_2Cl_2 at 298 K are listed in Table 2. For **1a–1d**, a

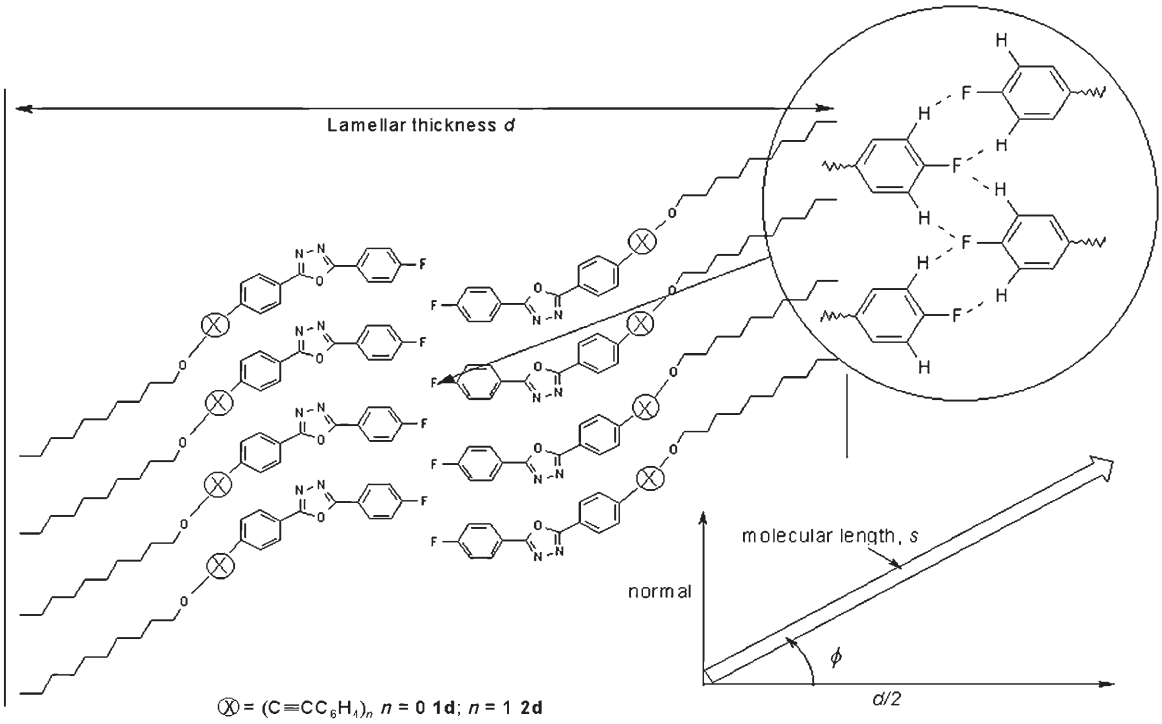

Scheme 2. Proposed lamellar structures of **1d** ($d \approx 37.6$ Å, $s \approx 23.5$ Å, $\phi \approx 37°$) and **2d** ($d \approx 47$ Å, $s \approx 30$ Å, $\phi \approx 37°$) based on the d values observed in their diffractograms.

Table 2. UV/Vis absorption and emission data for **1**–**3**.

Complex	λ_{max} [nm] (ε [dm^{3}mol^{-1}cm^{-1}])[a]	λ_{em} [nm] (τ [ns]) at 298 K[b]	Φ
1a	257 (15000), 304 (37000)	340 (sh, 1.14), 357 (max, 1.14), 371 (1.16)	0.78
1b	256 (12500), 303 (30400)	340 (sh, 1.15), 357 (max, 1.17), 371 (1.15)	0.83
1c	274 (sh, 13200), 338 (32600)	405 (1.40)	0.80
1d	246 (sh, 7170), 297 (27500)	363 (1.28)	0.73
2a	249 (sh, 20600), 264 (sh, 14000), 338 (47900)	401 (1.01)	0.89
2b	248 (sh, 18200), 265 (sh, 12900), 338 (49500)	401 (0.91)	0.97
2c	260 (17400), 282 (sh, 21500), 329 (sh, 37400), 359 (57200)	471 (2.60)	0.82
2d	334 (46400)	409 (1.00)	0.82
3a	259 (28150), 352 (78340)	417 (0.93)	0.84
3b	259 (25300), 350 (88000)	417 (0.93)	0.83

[a] In dichloromethane. [b] λ_{ex} at λ_{max} absorption, in dichloromethane at concentration $\approx 5 \times 10^{-6}$ M.

strong absorption band at $\lambda_{max} = 297$–338 nm ($\varepsilon = 27500$–37000 dm^{3}mol^{-1}cm^{-1}) and a weak absorption band at $\lambda_{max} = 246$–274 nm ($\varepsilon = 7170$–15000 dm^{3}mol^{-1}cm^{-1}) were observed. The lowest-energy absorption bands in **1a**–**1d** underwent a progressive red shift (F (**1d**) < $C_{10}H_{21}O$, CH_3O (**1a**, **1b**) < $N(CH_3)_2$ (**1c**)) as the electron-donating ability of their *para*-substituents was increased. The absorption spectra of **2a**–**2d** exhibited an intense absorption band at 334–359 nm ($\varepsilon = 4.6$–5.7×10^4 dm^{3}mol^{-1}cm^{-1}) and relatively weak shoulders at 248–329 nm ($\varepsilon = 1.3$–3.7×10^4 dm^{3}mol^{-1}cm^{-1}). Similarly, a strong absorption band centered at about 350 nm ($\varepsilon = 88000$–123000 dm^{3}mol^{-1}cm^{-1}) and a shoulder at $\lambda_{max} = 259$ nm ($\varepsilon = 25300$–35900 dm^{3}mol^{-1}cm^{-1}) were observed for **3a** and **3b**. The energy of the lowest absorption band in **2a**–**2d** was lowered by 1810–3730 cm^{-1} when a phenylethynyl ($C_6H_4C{\equiv}C$) unit was inserted between the oxadiazole and phenyl-ring moieties of the parent congeners **1a**–**1d**. In contrast, **3a** and **3b** displayed a slight red shift of about 1100 cm^{-1} for their lowest absorption bands at 350 nm, despite the fact that they have two additional phenylethynyl units. However, the ε value at $\lambda_{max} = 352$ nm for **3a** is the largest of the compounds studied in this work. All compounds were emissive at $\lambda_{max} = 357$–471 nm with emission quantum yields and lifetimes of 73–97% and 0.91–2.60 ns, respectively, in CH_2Cl_2 solution at 298 K. Notably, the Stokes shifts in the range of 4430–6120 cm^{-1}, which were measured for all these compounds except **2c**, are comparable to those found for 2,5-diphenyl-1,3,4-oxadiazole derivatives.[23] The largest Stokes shift was observed for **2c** ($\approx$6550 cm^{-1}), which may be explained by a "push–pull effect" created by the strong electron-donating $N(CH_3)_2$ group and the electron-accepting oxadiazole ring.

Liquid-Crystal Properties

The thermotropic liquid-crystalline behavior of the 2,5-disubstituted 1,3,4-oxadiazoles was studied by POM and DSC. The POM images of **1d**, **2a**, **2b**, and **2d** are shown in Figures 5–8, respectively. The phase-transition temperatures

CHEMISTRY
AN ASIAN JOURNAL

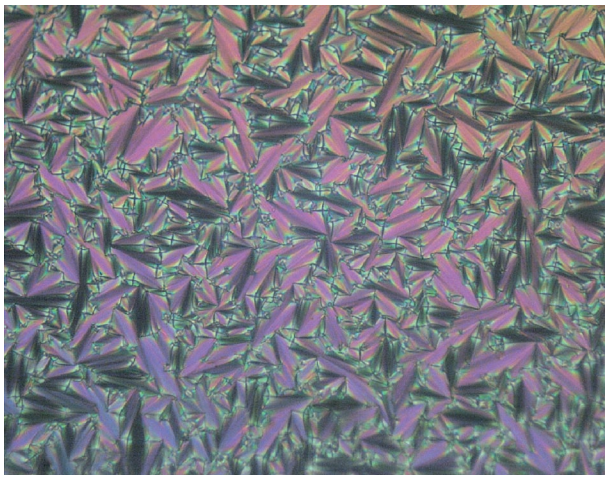

Figure 5. POM image of the Smectic A texture observed for **1d** obtained after heating the solid to 85 °C (magnification ×200).

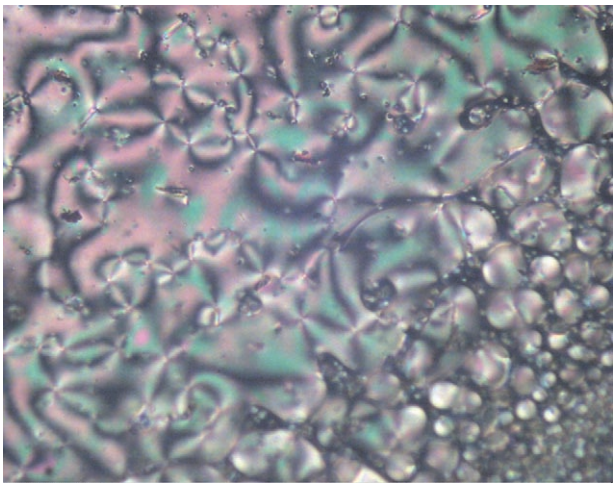

Figure 6. POM image showing the Schlieren texture of **2a** with four-brush singularities after the solid was heated to 115 °C (magnification ×200).

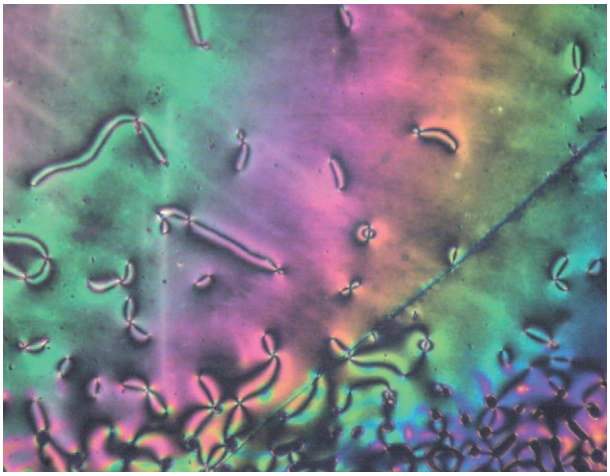

Figure 7. POM image of the Schlieren texture for **2b** with two- and four-brush singularities after the isotropic liquid was cooled to 116 °C (magnification ×200).

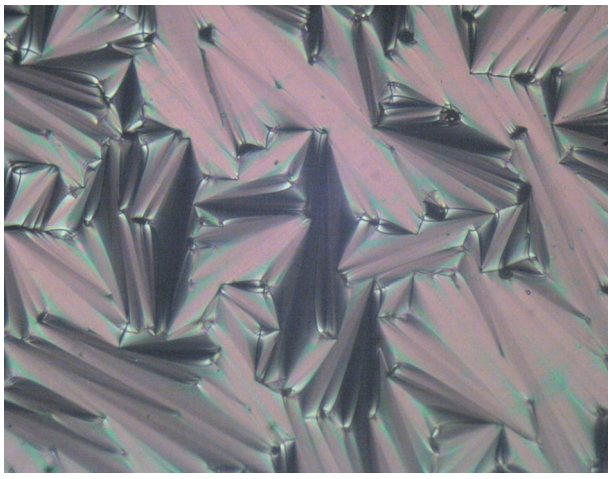

Figure 8. POM image of the Smectic A texture observed for **2d** obtained after the solid was heated to 183 °C (magnification ×200).

and enthalpy changes for the compounds were derived from the DSC measurements and are summarized in Table 3.

The formation of the mesophase was found to be affected by both electronic and steric factors within terminal substituents. For example, **1a**–**1c**, which contain electron-donating groups ($C_{10}H_{21}O$, CH_3O, and $(CH_3)_2N$), displayed no thermotropic liquid-crystalline properties. However, the solid **1d**, which contains *p*-fluoro substituents, produced an enantiotropic smectic A mesophase, which was confirmed

Table 3. Phase transitions for **1**–**3** calculated from DSC measurements.

Compound	Phase transition[a]	T [°C] (ΔH [kJ mol^{-1}])
1a	Cr1→I	123.8 (60.14)
1b	Cr1→Cr2	77.7 (17.82)
	Cr2→I	89.1 (3.41)
1c	Cr1→I	115.8 (38.26)
1d	Cr1→S_A	79.5 (16.28)
	S_A→I	86.1 (4.41)
2a[b]	Cr1→Cr2	116.1 (7.92)
	Cr2→N	131.6 (23.1)
	N→I	156.3 (0.67)
2b	Cr1→Cr2	112.34 (9.23)
	Cr2→I	137.6 (37.25)
	I→N	[126][c]
	N→Cr1	[103][c]
2c	Cr1→Cr2	51.5 (3.43)
	Cr2→Cr3	142.4 (9.28)
	Cr3→I	162.5 (25.15)
	I→N	[148][c]
	N→Cr4	[136][c]
2d	Cr1→Cr2	75.3 (3.66)
	Cr2→S_A	180.4 (30.17)
	S_A→I	202.5 (2.64)
3a[b]	Cr3→N	212.5 (51.8)
	N→I	234.8 (0.79)
3b	Cr1→I	255.1, decomposed

[a] Cr = crystal phase, N = nematic mesophase, S_A = smectic A mesophase, I = isotropic liquid. [b] See reference [11e]. [c] All I→N or N→Cr transition temperatures were not measured but based on POM observations.

by the observation of a focal conic texture in the POM image (Figure 5).[24] As the 2,5-diphenyl-1,3,4-oxadiazole and *p*-alkoxyphenyl moieties are electron-deficient and electron-rich, respectively, the incorporation of an electron-withdrawing F substituent into the molecule perturbs the charge distribution and produces a larger molecular dipole. Consequently, the net dipolar interactions among molecules stabilize the mesophase. In contrast, the electron-donating $(CH_3)_2N$ and CH_3O) substitutents destablize the mesophase, probably owing to the absence of dipolar interactions in these mesogens.

POM revealed that **2a** had a typical Schlieren texture,[25] which indicates an enantiotropic nematic mesophase (Figure 6), whereas a monotropic mesophase with a thread-like texture was observed[25] upon cooling the isotropic liquids **2b** and **2c** (Figure 7). In **2d**, an enantiotropic smectic A mesophase was confirmed by the typical fan-shaped texture as shown in Figure 8. Notably, the more-extended mesogens **2a**–**2d** could readily form thermotropic mesophases, in contrast to the analogues **1a**–**1d**. This observation may be explained by an increase in the π conjugation between the phenyl and ethynyl moieties. The mesogenic character of **2a**–**2d** is greater than that of **1a**–**1d**, as a result of extended π conjugation, due to the presence of additional phenylethynyl entities. Thus, **3a** exhibits an enantiotropic nematic mesophase, and **3b** has no mesomorphic behavior. Molecule **3b** is rigid with no mesogenic flexibility, owing to the absence of long terminal *n*-alkyl chains. In summary, a higher length-to-breadth ratio for these mesogenic molecules enhances the stability of the parallel molecular aggregations in the liquid-crystal state. The liquid-crystal properties of extended 2,5-disubstituted-1,3,4-oxadiazole derivatives may be readily modified by including different terminal groups and changing the lengths of the conjugated mesogenic cores.

Thermogravimetric Analysis

The relative thermal stability of the mesogenic materials **1b, 1d**, **2b, 2d**, and **3a** was investigated by thermogravimetric analysis (TGA). The TGA curves of these solids recorded at 25–700 °C under N_2 atmosphere are included in the Supporting Information. Only in the case of **1b** was there a weight loss of 2% at 25–80 °C, which was attributed to the loss of 0.5 molar equivalents of occluded H_2O molecules per formula-mass unit. All the solids decomposed by a two-step process and showed different onset decomposition temperatures (200 °C for **1b**, 235 °C for **1d**, 280 °C for **2b**, 285 °C for **2d**, 335 °C for **3a**). These temperatures increased with the molecular weight of the mesogen. For **1b** and **1d**, the replacement of the terminal methoxy group with a fluoro substituent led to an increase in the onset temperature, which was attributed to lattice stabilization through the formation of intermolecular C–H···F–C interactions. However, this did not occur for the extended analogues **2b** and **2d**. All the solids were thermally stable with insignificant weight losses below 200 °C. However, the results of the in situ VTXRD studies described below reveal that various crystal-to-crystal and crystal-to-mesophase transitions occurred when the solid samples were heated from 25 to 200 °C.

In situ Variable-Temperature X-ray Diffraction

The structural changes associated with the crystalline solids and mesophases were monitored by in situ VTXRD. The relevant diffractograms of solids **1b**, **1d**, **2b**, **2d**, and **3a** are shown in Figures 9–13, respectively. For **1b**, a crystal-to-crys-

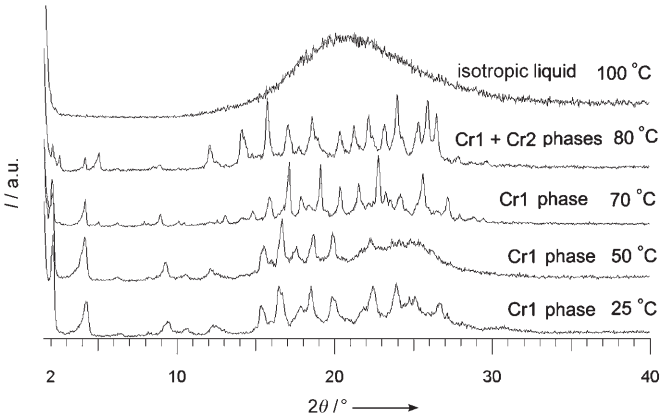

Figure 9. Variable-temperature diffractograms of **1b** at 25–100 °C.

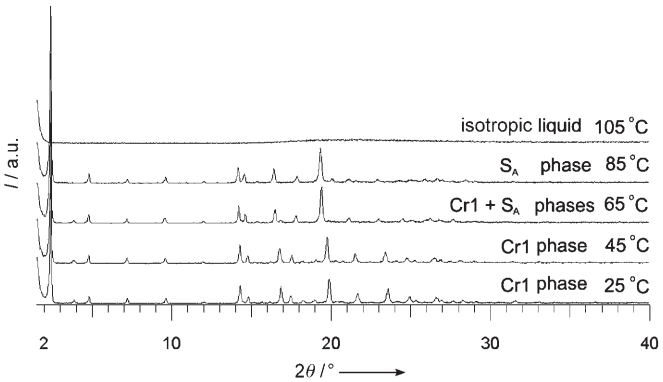

Figure 10. Variable-temperature diffractograms of **1d** at 25–105 °C.

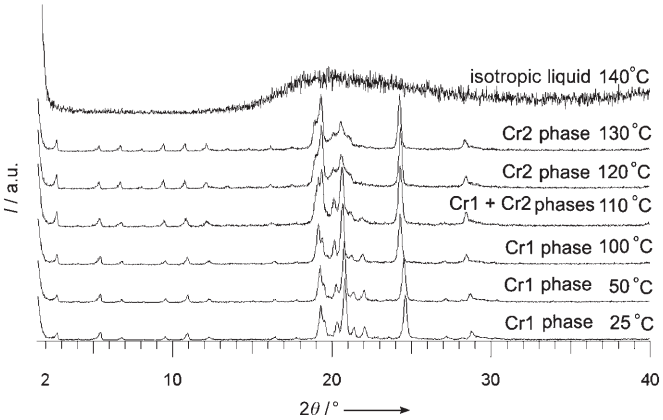

Figure 11. Variable-temperature diffractograms of **2b** at 25–140 °C.

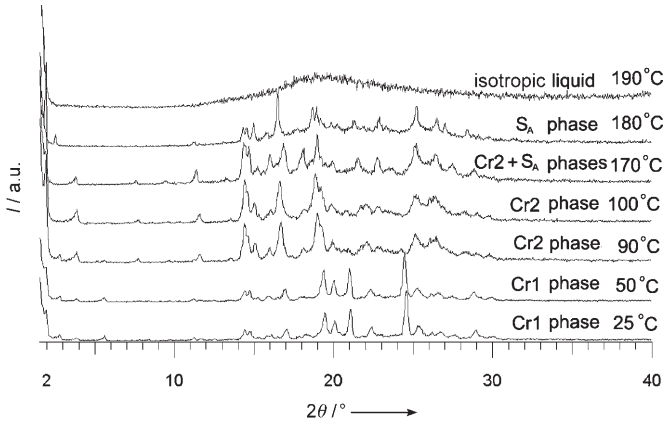

Figure 12. Variable-temperature diffractograms of **2d** at 25–190 °C.

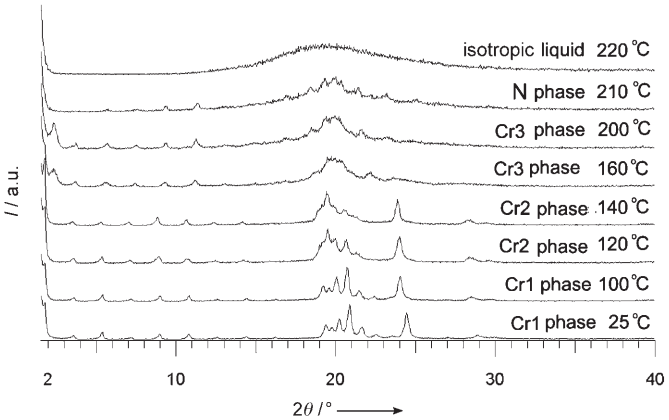

Figure 13. Variable-temperature diffractograms of **3a** at 25–220 °C.

tal transition (Cr1→Cr2) occurred between 70 and 80 °C, as evidenced by the appearance of two additional diffraction peaks at 2.50° and 4.97° (2θ) in the diffractogram recorded at 80 °C (Figure 9). In line with the POM and DSC results, the two crystal polymorphs of **1b** (Cr1 and Cr2) coexisted without forming any mesophase. These two crystal polymorphs completely melted to form an isotropic liquid at 100 °C. Upon cooling the sample to 25 °C, the ^{1}H NMR spectrum of the annealed solid residue showed that the chemical structure remained unchanged. There was no such crystal-to-crystal transition for **1d** at 25–45 °C, as the relative intensity and peak positions of the first five diffraction peak maxima remained unchanged. At 65 °C, a new phase appeared, and a small amount of crystalline phase was present. Well-defined periodic peak maxima [q, $2q$, $3q$, $4q$, $5q$, $6q$, $7q$, $8q$; q/Å^{-1}(2θ/°): 0.041 (2.345), 0.083 (4.751), 0.125 (7.168), 0.166 (9.591), 0.208 (12.007)] were noted at 65 °C (Figure 10), thus indicating that this new phase is a smectic A mesophase whose formation was complete at 85 °C. The lamellar thickness (37.7 Å) of this mesophase is almost identical to that which appeared in the crystalline solid **1d** at room temperature. The diffractograms of **2b** at 25–130 °C closely resembled each other except in the 2θ region at 19–23°, at 100–110 °C (Figure 11). DSC measurements indicate a phase transition at 108–117 °C, but the POM study suggests that a monotropic nematic mesophase was only formed when the isotropic liquid was cooled to 126 °C. We attributed this change in the diffractograms between 100 and 120 °C to a crystal-to-crystal transition. Thus, the peak maxima [q, $2q$, $2.5q$, $3q$, $3.5q$, $4q$; q/Å^{-1}(2θ/°): 0.046 (2.655), 0.093 (5.316), 0.116 (6.664), 0.140 (8.042), 0.163 (9.379)] that appeared at 130 °C came from another crystal polymorph (Cr2). The relative intensity and peak shape of the two high-angle peaks at 24.5° and 28.8° (2θ; corresponding to the molecular width (3.7 Å) and typical molecular π···π stacks (3.2 Å), respectively) in the two crystal polymorphs are almost unaltered, indicating a structural resemblance. Somewhat surprisingly, the diffractograms for the crystalline solid **2b** and the corresponding annealed residue were practically identical to each other, as shown in the Supporting Information. The lateral molecular order increased remarkably in the annealed sample, as the intensity of the diffraction peak at 24.5° (2θ) was approximately doubled. On the contrary, more-complicated phase transitions were observed for the solids **2d** and **3a**. These phase transitions can be collectively described by the multistep process Cr1→Cr2→S_A (or Cr3→N for **3a**)→I. For **2d**, a crystal-to-crystal transition (Cr1→Cr2) occurred between 50 and 90 °C (Figure 12). The POM and DSC results indicate that a new phase, with a lamellar thickness of 35.8 Å, appeared at 180 °C, which is attributed to the smectic mesophase of **2d**. Two notable phase transitions were found for **3a** between 100 and 120 °C as well as between 140 and 160 °C (Figure 13). These transitions were assigned to Cr1→Cr2 and Cr2→Cr3 crystal-to-crystal transitions, respectively, and POM confirmed that no mesophase was formed within this temperature range. As the solid **3a** was further heated to 210 °C, the low-angle peak at 2.56° (2θ) completely disappeared before the solid quickly melted. We believe that a transient enantiotropic nematic mesophase was formed at about 205 °C, which is consistent with the observations of overlapping DSC peaks and the POM results.

Small-Angle X-ray Scattering

The long-range molecular order for these extended mesogenic molecules, both before and after annealing, was further investigated by powder SAXS. Figure 14 shows the SAXS patterns of the scattered signals in an angular range of $<3°$ (2θ). The long-range order was only preserved in solid **2b** after annealing at 140 °C. The SAXS patterns indicate that upon cooling the isotropic liquids to room temperature, **1b**, **2d**, and **3a** recrystallized into different types of crystal polymorphs (a mixture of Cr1 and Cr2 for **1b**, Cr2 for **2d**, Cr3 for **3a**). However, the long-range order in the crystalline solid **1d** completely vanished after annealing.

Structure–Property Relationships

Herein, all the mesogenic molecules possess 1) the same ether oxygen linkage between the rigid 2,5-disubstituted-

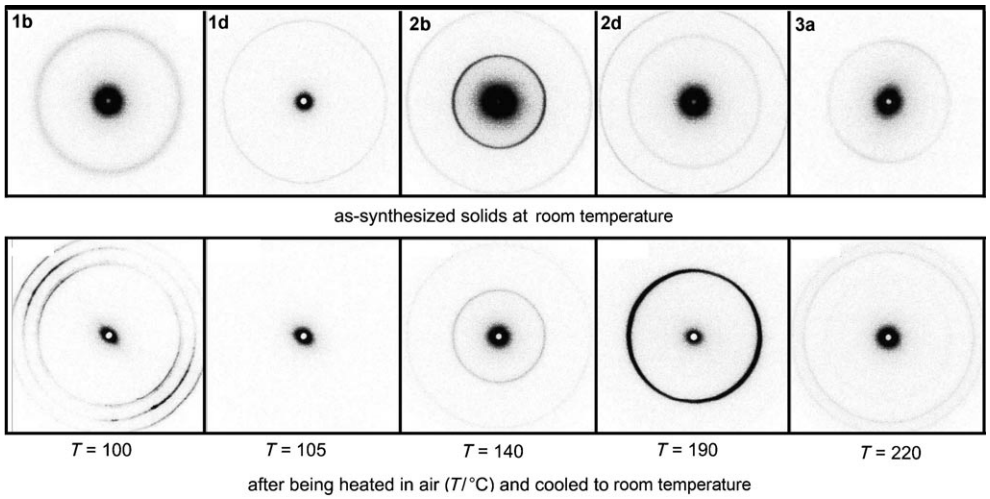

Figure 14. SAXS patterns for the crystalline solids **1b**, **1d**, **2b**, **2d**, **3a** (upper), and their annealed solid residues (lower). The angular positions 2θ (°) of the scattered signals were: **1b**: 2.166 (upper) and 2.162, 2.561, 2.932 (lower); **1d**: 2.376 (upper) and 0 (lower); **2b**: 1.386, 2.673 (upper) and 1.359, 2.653 (lower); **2d**: 1.977, 2.933 (upper) and 2.050 (lower); **3a**: 1.974 (upper) and 2.470, 2.790 (lower).

1,3,4-oxadiazole moieties and the flexible *n*-decyl chains and 2) no lateral side group. The formation of a mesophase is solely attributed to the different mesogenic core lengths as well as the electronic properties of the terminal substituents. The rodlike mesogenic molecules **1d**, **2a**–**2d**, and **3a** exhibited typical nematic and smectic mesophases, whereas discotic (disklike) mesogens usually produce various columnar mesophases. For example, Lai et al. reported the liquid-crystal properties of heterocyclic 2,5-bis(3,4,5-trialkoxyphenyl)-1,3,4-oxadiazoles[11a] (L) and the metallomesogens $[L_2PdCl_2]$.[11d] The formation of their columnar mesophases was strongly dependent on the size as well as the number of appended alkoxy substituents. These crystalline solids underwent crystal-to-mesophase transitions at lower temperatures (30–54.4 °C) than those (64–170 °C) for **1d**, **2a**, and **3a**. The incorporation of lateral NO_2 groups into **2a** and **3a** reduced the onset temperatures for the crystal-to-mesophase transition and induced new types of smectic mesophases.[11e] The effects of incorporating lateral alkoxy groups of 1,4-bis(5-alkoxyphenyl-1,3,4-oxadiazolyl)benzene on the liquid-crystal properties and transient smectic-to-nematic mesophase transitions have already been reported.[11b]

For **1a**–**1c**, the mesogenic core lengths of the 2,5-diphenyl-1,3,4-oxadiazole moieties are 12–14 Å; it is thus difficult for them to form any mesophase. From our structural analyses, the solid **1d** probably has a tilted bilayer structure, presumably due to intermolecular C–H···F–C interactions between adjacent stacks of molecules. As diffraction peaks near 24° and 28° (2θ) were not found, C–H···π and π···π interactions in the crystalline solid **1d** are not apparent. Therefore, C–H···F–C interactions are important for the stabilization of the lamellar structure in the crystalline solid as well as in the smectic mesophase. The effect of polar substituents of 2-(*n*-decyloxy)-5-(naphthalen-2-yl)-1,3,4-oxadiazoles (10-NPO-X; X = *p*-$CH_3C_6H_4$, *p*-$CH_3OC_6H_4$, *p*-FC_6H_4, *p*-ClC_6H_4, *p*-$N{\equiv}CC_6H_4$, *p*-$NO_2C_6H_4$) on liquid-crystal behavior has previously been reported.[11c] In this case, nematic mesophases were only observed when the terminal substituents are *p*-tolyl and *p*-methoxyphenyl, whereas the mesogens containing *para*-F, Cl, CN, and NO_2 substituents formed well-ordered smectic mesophases. These earlier findings were attributed to the larger molecular dipole moments of these electron-withdrawing substituents, as well as the possible formation of intermolecular C–H···X hydrogen bonds (X = F, Cl, N≡C, and O–NO).

The insertion of phenylethynyl unit(s) into molecules **1a**–**1d** afforded the extended analogues **2**–**3**, which have larger molecular length-to-breath ratios. This structural modification not only alters the emission/absorption spectra of the compounds, but also enhances the molecular rigidity as well as the formation of intermolecular C–H···π and/or π···π interactions. Powder XRD studies revealed that the solids **2b**, **2d**, and **3a** had two prominent diffraction peaks at 2θ near 24–25° (d = 3.8–3.7 Å) and 28–29° (d = 3.2–3.3 Å), revealing the presence of lateral molecular order stabilized by intermolecular C–H···π and/or π···π interactions. Subsequently, we found that their melting points increased and their solubility decreased relative to the parent molecules **1a**–**1d**. For **2a**–**2d**, the mesophases were stabilized by increased mesogenic character due to the additional phenylethynyl moieties. Depending on their terminal substituents, either nematic or smectic mesophases were formed. In **2a**–**2c**, the terminal substituents are relatively electron-donating and preferentially lead to enantiotropic or monotropic nematic-mesomorphic behavior. This is in contrast to the smectic mesophase of **2d**, which contains an electron-withdrawing F substituent. The addition of one phenylethynyl moiety further increases the mesogenic character of **3a**, leading to a higher onset temperature for the crystal-to-mesophase transition (from 131 to 212.5 °C). Similarly, it was previously shown that the incorporation of a bis(1,3,4-oxadiazole) unit together with an *m*-phenylene[11e] spacer in the mesogenic core also led to

increases in the onset temperature for the crystal-to-mesophase transition (212.5 °C for **3a**, 258 °C for 1,3-$[C_{10}H_{21}OC_6H_4(C{\equiv}C)C_6H_4\{C_2N_2O\}]_2C_6H_4$). However, when the two *n*-decyl chains were replaced with methoxy groups, as in **3b**, decomposition occurred without the formation of a mesophase.

Besides the molecular structures, we also considered the effect of crystal packing on the formation of mesomorphic structures. Based on the solid-state structures of **2b** and **3a**, which were solved by powder XRD, sliding these rodlike molecules along their long crystallographic axes leads to three possible structural-transformation pathways (Scheme 3). Depending on the relative strengths of the mesogen–mesogen and chain–chain interactions in the solid state, either the smectic or the nematic mesophase may be obtained. For **1d** and **2d**, the molecules form a lamellar-like structure with both positional and orientational order, whereas only orientational order exists in the case of **2b** and **3a**. This suggests that if the mesogen–mesogen interactions (e.g., C–H···F–C in **1d** and **2d**) are stronger and dominate

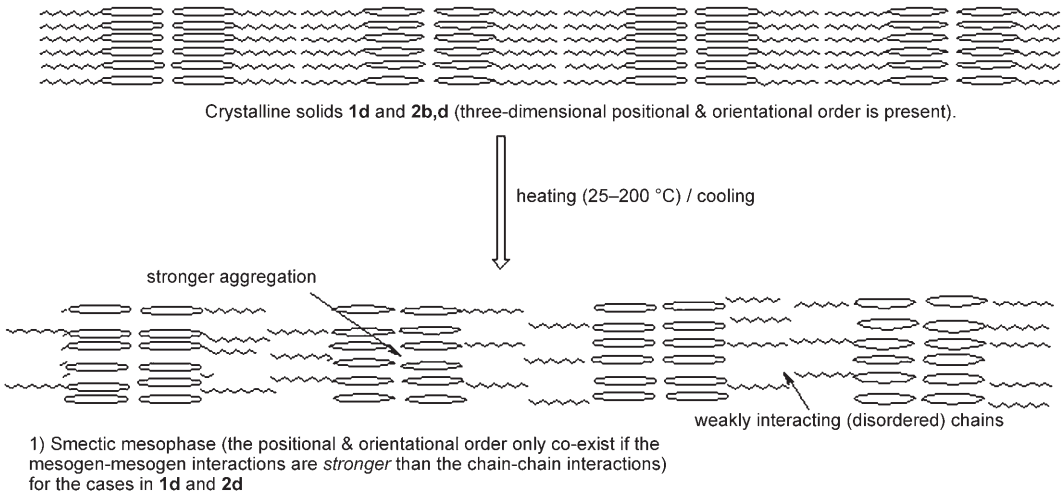

Scheme 3. Schematic representation of possible solid-to-mesophase transition pathways for **1d**, **2b**, **2d**, and **3a** based on the crystal packing of **2b** and **3a**.

in the crystal structure, the smectic mesophase is preferred. Otherwise, either a monotropic or enantiotropic nematic mesophase is formed due to 1) entropic reasons and/or 2) similar bond strengths for the mesogen–mesogen and chain–chain interactions (Scheme 3).

Conclusions

A new class of extended 2,5-disubstituted-1,3,4-oxadiazoles were prepared, and their liquid-crystal properties were investigated by using various techniques. Upon heating/cooling, the crystalline solids exhibited nematic or smectic mesophases, depending on their mesogenic core length and the terminal substituents. We found that an increase in the mesogenic character of the calamitic (rodlike) molecules favored the stabilization of the mesophase. The electronic properties of the terminal substituents could significantly alter the nature of the mesophase, which could also be influenced by crystal/molecular packing and intermolecular interactions.

Experimental Section

All starting materials were commercially available and used as received. The solvents used were of analytical grade. Benzene, tetrahydrofuran, and dichloromethane were predried and distilled over sodium in benzophenone or calcium hydride.[12] Elemental analyses were performed by the Institute of Chemistry, the Chinese Academy of Sciences. UV/Vis spectra were recorded on a Perkin–Elmer Lambda 19 UV/Vis spectrophotometer. Steady-state emission spectra were recorded on a SPEX Fluorolog-II Model F111 spectrophotometer. Solution samples for measurements were degassed with at least four freeze–pump–thaw cycles. The emission spectra were corrected for monochromator and photomultiplier efficiency and for xenon lamp stability. Emission lifetime measurements were performed with a Quanta Ray DCR-3 pulsed Nd/YAG laser system. Errors for λ ($\pm$1 nm), τ ($\pm$10%), and Φ ($\pm$10%) were estimated. Emission quantum yields were determined by using the method of Demas and Crosby[13] with quinine sulfate in sulfuric acid (0.1 N) as a standard reference solution (Φ_r=0.546). ^{1}H and ^{13}C-{^{1}H} NMR spectra were collected on Bruker AVANCE 300/400 MHz DRX FT-NMR spectrometers. Electron impact (EI) and high-resolution mass spectra (HRMS) were recorded by a Finnigan MAT 95 mass spectrometer. The liquid-crystalline behavior of all compounds was studied on a polarized-light optical microscope equipped with a heating stage. The thermal properties of the bulk materials were studied by using a Perkin–Elmer DSC-7a differential scanning calorimeter with a heating rate of 10 °C min^{-1}, precalibrated with an indium standard (156.6 °C, 3.3 kJ mol^{-1}). TGA of solids **1b**, **1d**, **2b**, **2d**, and **3a** were performed with a Perkin–Elmer TGA-7 instrument under a stream of flowing N_2.

Step-scanned powder XRD data of **1b**, **1d**, **2b**, **2d**, and **3a** were collected at room temperature on a Bruker D8 ADVANCE diffractometer (θ/θ geometry) with parallel X-ray radiation ($Cu_{K\alpha}$, λ=1.5418 Å, rated at 1.6 kW) by using a multilayer Göbel mirror. The in situ variable-temperature X-ray diffractograms were recorded with a modular temperature chamber attachment (Materials Research Instruments) in the temperature range 25–300 °C at reduced pressure. Scan range = 1.5–40° (2θ), step size = 0.02°, scan time = 1 s per step. The zero-point peak shift error of 0.05° (2θ) of the X-ray diffractometer was calculated by the strongest peak of the standard silicon {111} single crystal at 28.467° (2θ). For the structure determination of **2b** and **3a**, phase-pure powder samples prepared by repeated mechanical grinding were side-loaded onto a flat standard sample holder (10 × 10 mm^2). Overnight data acquisition was conducted at a scan speed of 10 s per step on a Philips PW3710 diffractometer ($\theta/2\theta$ geometry). The instrumental broadening parameters and geometrical constants (S/L and H/L values) of the diffractometer were evaluated by structural refinement of the peak-shape standard LaB_6 (NIST 660a). Details of the structure determination of **2b** and **3a** are described in the Supporting Information.

SAXS data were acquired on a Bruker NANOSTAR U system with a ceramic sealed X-ray tube ($Cu_{K\alpha}$, λ=1.5418 Å, rated at 1.2 kW). The divergent X-ray was prealigned by two multilayer Göbel mirrors oriented in the horizontal and vertical directions. The incident X-ray beam (0.6 × 0.6 mm^2) was collimated by three pinholes, and the solid sample was mounted on an adhesive tape (Scotch 3M). Positioning of the sample holder was driven by a computer-controlled gonoimeter. Data collection was carried out in a sealed sample chamber under a dynamic vacuum of 2×10^{-3} mbar. The scattering signal was measured by a 2D position-sensitive gas detector (HI-STAR). The sample-to-detector distance (1050 mm) was precalibrated by using the d value of the first-order diffraction ring (2θ = 1.514°, d = 58.354 Å) of a silver behenate ($C_{21}H_{43}CO_2Ag$) standard. The raw scattering data was corrected for intensity variations due to spatial aberrations and nonuniformity of the 2D detector. The peak maxima of the scattered signal were automatically determined by radial integration along the chi direction (2θ range = 1.0–3.0°, chi-angle range = 0–355°) of the scattering pattern. The results were plotted as normalized intensity versus scattering angle (I vs. 2θ) with the SAXS NT (Bruker AXS) program.[14]

Acknowledgements

S.S.-Y.C. acknowledges a postdoctoral fellowship from The University of Hong Kong as well as support from the University Development Fund (UDF) through the HKU Nanotechnology Research Institute Program and the Strategic Research Team on Organic Optoelectronics.

[1] a) B. Bahadur, *Mol. Cryst. Liq. Cryst.* **1984**, *109*, 1–93; b) M. Schadt, *Displays* **1992**, *13*, 11–33; c) C. Booth, P. Raynes, *Physics World* **1997**, *10*, 33–37; d) G. W. Gray, S. M. Kelly, *J. Mater. Chem.* **1999**, *9*, 2037–2050.

[2] a) L. Dinescu, K. E. Maly, R. P. Lemieux, *J. Mater. Chem.* **1999**, *9*, 1679–1686; b) T. Ikeda, A. Kanazawa, *Bull. Chem. Soc. Jpn.* **2000**, *73*, 1715–1733; c) V. Y. Zyryanov, E. P. Pozhidaev, S. L. Smorgon, A. L. Andreev, D. Ganzke, V. F. Shabanov, I. N. Kompanets, W. Haase, *Liq. Cryst.* **2001**, *28*, 741–748; d) M. Frigoli, G. H. Mehl, *Chem. Eur. J.* **2004**, *10*, 5243–5250.

[3] a) M. Frigoli, G. H. Mehl, *Eur. J. Org. Chem.* **2004**, 636–642; b) Q. Li, L. Li, J. Kim, H. S. Park, J. Williams, *Chem. Mater.* **2005**, *17*, 6018–6021.

[4] a) M. F. Schiekel, K. Fahrensc, *Appl. Phys. Lett.* **1971**, *19*, 391–393; b) G. Labrunie, J. Robert, *J. Appl. Phys.* **1973**, 144, 4869–4874; c) S. Matsumoto, M. Kawamoto, K. Mizunoya, *J. Appl. Phys.* **1976**, *47*, 3842–3845.

[5] G. Lüssem, J. H. Wendorff, *Polym. Adv. Technol.* **1998**, *9*, 443–460.

[6] a) S. Bonazzi, M. M. Demorais, G. Gottarelli, P. Mariani, G. P. Spada, *Angew. Chem.* **1993**, 105, 251–254; *Angew. Chem. Int. Ed. Engl.* **1993**, *32*, 248–250; b) F. Ciuchi, G. Dinicola, H. Franz, G. Gottarelli, P. Mariani, M. G. Ponzi Bossi, G. P. Spada, *J. Am. Chem. Soc.* **1994**, *116*, 7064–7071; c) V. Reiffenrath, M. Bremer, *Angew. Chem.* **1994**, *106*, 1435–1438; *Angew. Chem. Int. Ed. Engl.* **1994**, *33*, 1386–1389.

[7] a) J. M. Lehn, *Angew. Chem.* **1990**, *102*, 1347–1362; *Angew. Chem. Int. Ed. Engl.* **1990**, *29*, 1304–1319; b) T. Kato, H. Kihara, U. Kumar, T. Uryu, J. M. J. Fréchet, *Angew. Chem.* **1994**, *106*, 1728–1730; *Angew. Chem. Int. Ed. Engl.* **1994**, *33*, 1644–1645; c) L. Brunsveld, B. J. B. Folmer, E. W. Meijer, R. P. Sijbesma, *Chem. Rev.* **2001**, *101*, 4071–4097; d) M. Lee, B.-K. Cho, W. C. Zin, *Chem. Rev.* **2001**, *101*, 3869–3892; e) R. Ziessel, *Coord. Chem. Rev.* **2001**, *216*, 195–223; f) J. L. Serrano, T. Sierra, *Coord. Chem. Rev.* **2003**, *242*, 73–85;

g) F. J. M. Hoeben, P. Jonkheijm, E. W. Meijer, A. P. H. J. Schenning, *Chem. Rev.* **2005**, *105*, 1491–1546; h) H. M. Keizer, R. P. Sijbesma, *Chem. Soc. Rev.* **2005**, *34*, 226–234; i) S. Kumar, *Chem. Soc. Rev.* **2006**, *35*, 83–109.

[8] a) Q. Pei, Y. Yang, *Chem. Mater.* **1995**, *7*, 1568–1575; b) J. Bettenhausen, P. Strohriegl, *Adv. Mater.* **1996**, *8*, 507–510; c) W. Huang, H. Meng, W. L. Yu, J. Gao, A. J. Heeger, *Adv. Mater.* **1998**, *10*, 593–596; d) W. L. Yu, H. Meng, J. Pei, W. Huang, Y. F. Li, A. J. Heeger, *Macromolecules* **1998**, *31*, 4838–4844; e) B. Verheyde, W. Dehaen, *J. Org. Chem.* **2001**, *66*, 4062–4064; f) X. W. Zhan, Y. Q. Liu, X. Wu, S. A. Wang, D. B. Zhu, *Macromolecules* **2002**, *35*, 2529–2537; g) K. L. Paik, N. S. Baek, H. K. Kim, J. H. Lee, Y. Lee, *Opt. Mater.* **2003**, *21*, 135–142; h) F. I. Wu, D. S. Reddy, C. F. Shu, M. S. Liu, A. K. Y. Jen, *Chem. Mater.* **2003**, *15*, 269–274; i) N. P. Tzanetos, J. K. Kallitsis, *Chem. Mater.* **2004**, *16*, 2648–2655.

[9] a) C. Adachi, S. Tokito, T. Tsutsui, S. Saito, *Jpn. J. Appl. Phys. Part 2* **1988**, *27*, L713–L715; b) Y. Hamada, C. Adachi, T. Tsutsui, S. Saito, *Jpn. J. Appl. Phys. Part 1* **1992**, *31*, 1812–1816.

[10] B. Schulz, I. Orgzall, A. Freydank, C. Xu, *Adv. Colloid Interface Sci.* **2005**, 116, 143–164.

[11] a) C. K. Lai, Y. C. Ke, J. C. Su, C. Shen, W. R. Li, *Liq. Cryst.* **2002**, 29, 915–920; b) D. Acierno, S. Concilio, A. Diodati, P. Iannelli, S. P. Piotto, P. Scarfato, *Liq. Cryst.* **2002**, 29, 1383–1392; c) H. H. Sung, H. C. Lin, *Liq. Cryst.* **2004**, *31*, 831–840; d) C. R. Wen, Y. J. Wang, H. C. Wang, H. S. Sheu, G. H. Lee, C. K. Lai, *Chem. Mater.* **2005**, *17*, 1646–1654; e) R. Cristiano, F. Ely, H. Gallardo, *Liq. Cryst.* **2005**, 32, 15–25.

[12] D. D. Perrin, W. L. F. Armarego, D. R. Perrin, *Purification of Laboratory Chemicals*, *1st ed.*, Pergamon Press Ltd., **1966**.

[13] J. N. Demas, G. A. Crosby, *J. Phys. Chem.* **1971**, *75*, 991–1024.

[14] Small-Angle X-ray Scattering (SAXS) Version 4.0 Software Reference Manual NT, Bruker Advanced X-ray Solutions Inc., Madison, WI, **2000**.

[15] F. N. Hayes, B. S. Rogers, D. G. Ott, *J. Am. Chem. Soc.* **1955**, *77*, 1850–1852.

[16] a) S. Takahashi, Y. Kuroyama, K. Sonogashira, N. Hagihara, *Synthesis* **1980**, 627–630; b) K. Sonogashira in *Handbook of Organopalladium Chemistry for Organic Synthesis*, *Vol. 1* (Eds.: E. Negishi, A. de Meijere), **2002**, pp. 493–529.

[17] a) L. El Kaim, I. Le Menestrel, R. Morgentin, *Tetrahedron Lett.* **1998**, *39*, 6885–6888, and references therein; b) J. Sauer, R. Huisgen, H. J. Sturm, *Tetrahedron* **1960**, *11*, 241–251.

[18] a) S. W. Cha, S. H. Choi, K. Kim, J. I. Jin, *J. Mater. Chem.* **2003**, *13*, 1900–1904; b) C. S. Wang, A. S. Batsanov, M. R. Bryce, *Chem. Commun.* **2004**, 578–579.

[19] a) P. F. H. Schwab, M. D. Levin, J. Michl, *Chem. Rev.* **1999**, *99*, 1863–1933; b) P. Nguyen, P. Gómez-Elipe, I. Manners, *Chem. Rev.* **1999**, *99*, 1515–1548; c) U. H. F. Bunz, Y. Rubin, Y. Tobe, *Chem. Soc. Rev.* **1999**, *28*, 107–119; d) N. J. Long, C. K. Williams, *Angew. Chem.* **2003**, *115*, 2690–2722; *Angew. Chem. Int. Ed.* **2003**, *42*, 2586–2617; e) M. B. Nielsen, F. Diederich, *Chem. Rev.* **2005**, *105*, 1837–1867.

[20] Crystal data for **IIIc**: $C_{16}H_{14}IN_3O$, $M_r = 391.20$, orthorhombic, *Pbca*, $a = 12.409(3)$, $b = 10.678(2)$, $c = 23.592(5)$ Å, $V = 3126.0(11)$ Å^3, $Z = 8$, $T = 301$ K, $\rho_{calcd} = 1.662$ g cm^{-3}, $\mu_{Mo} = 2.051$ mm^{-1}, $F(000) = 1536$, total number of observed $[F^2 > 2\sigma(I)]$ and independent reflections = 2477 ($R_{int} = 0.054$), number of parameters = 190, $R1 = 0.030$, $wR2 = 0.066$. Crystal data for **Vc**: $C_{18}H_{17}N_3O_2$, $M_r = 307.35$, monoclinic, $P2_1/n$, $a = 10.679(2)$, $b = 13.893(3)$, $c = 10.700(2)$ Å, $\beta = 91.66(3)°$, $V = 1586.8(5)$ Å^3, $Z = 4$, $T = 253$ K, $\rho_{calcd} = 1.286$ g cm^{-3}, $\mu_{Mo} = 0.086$ mm^{-1}, $F(000) = 648$, total number of observed $[F^2 > 2\sigma(I)]$ and independent reflections = 2574 ($R_{int} = 0.053$), number of parameters = 216, $R1 = 0.048$, $wR2 = 0.109$. CCDC-602981 (**IIIc**) and -602982 (**Vc**) contain the supplementary crystallographic data (excluding structure factors) for this paper. These data can be obtained free of charge from the Cambridge Crystallographic Data Centre, 12 Union Road, Cambridge CB2 1EZ, UK (fax: (+44) 1223–336–033; e-mail: deposit@ccdc.cam.ac.uk) or at www.ccdc.cam.ac.uk/data_request/cif. Intensity data were collected with an MAR diffractometer with a 300-mm image plate detector using graphite-monochromated $Mo_{K\alpha}$ radiation ($\lambda = 0.71073$ Å). Structures were solved by direct methods with the SHELXS-97 program[26] on a PC. Most of the non-hydrogen atoms were located in this way. The positions of the remaining non-hydrogen atoms were found after successful refinement by full-matrix least-squares with SHELXL-97 on a PC.[26] The crystallographic asymmetric unit consists of one formula unit. In the final stage of least-squares refinement, all non-hydrogen atoms were refined anisotropically for both structures. The positions of H atoms were calculated as a riding model with isotropic thermal parameters equal to 1.2 times that of the attached C atoms and were included for the calculations of the final *R* indices.

[21] a) A. N. Parikh, S. D. Gillmor, J. D. Beers, K. M. Beardmore, R. W. Cutts, B. I. Swanson, *J. Phys. Chem. B* **1999**, *103*, 2850–2861 (the size of methylene unit is 1.20 Å for silver *n*-alkylthiolates); b) K. Binnemans, R. V. Deun, B. Thijs, I. Vanwelkenhuysen, I. Geuens, *Chem. Mater.* **2004**, *16*, 2021–2027. (that of silver *n*-alkanoates is 1.25 Å).

[22] a) J. N. Low, B. Insuasty, H. Torres, J. Cobo, *Acta Crystallogr. Sect. E* **2003**, *59*, o1801–o1803; b) D. E. Lynch, I. McClenaghan, *Acta Crystallogr. Sect. E* **2002**, *58*, o731–o732; c) S. Thamotharan, V. Parthasarathi, R. Gupta, D. P. Jindal, A. Linden, *Acta Crystallogr. Sect. C* **2003**, *59*, o724–o726.

[23] D. L. Horrocks, *J. Chem. Phys.* **1969**, *50*, 4962–4966.

[24] G. W. Gray, J. W. Goodby, *Smectic Liquid Crystals: Textures and Structures*, Leonard Hill, Glasgow, **1984**.

[25] a) D. Demus, L. Richter, *Textures of Liquid Crystals*, Verlag Chemie, Weinheim, **1984**; b) I. Dierking, *Textures of Liquid Crystals*, Wiley-VCH, Weinheim, **2003**.

[26] G. M. Sheldrick, SHELX97 Programs for Crystal-Structure Analysis (Release 97-2), University of Göttingen (Germany), **1997**.

Received: August 3, 2006
Published online: November 10, 2006

